

Red sequence modal colour gradients across intermediate X-ray luminosity galaxy clusters

Peter C. Jensen^{1*} and Kevin A. Pimbblet^{2,3†}

¹Centre for Astrophysics and Supercomputing, Swinburne University of Technology, Hawthorn, Victoria 3122, Australia

²School of Physics, Monash University, Clayton, Victoria 3800, Australia

³Monash Centre for Astrophysics (MoCA), Monash University, Clayton, Victoria 3800, Australia

DRAFT: 1 MARCH 2018 — DO NOT DISTRIBUTE

ABSTRACT

We assemble a sample of 45 intermediate X-ray luminosity galaxy clusters ($0.7 \times 10^{44} < L_X < 4 \times 10^{44}$ ergs⁻¹) at low redshifts ($0.03 < z < 0.16$) using SDSS data to conduct a comprehensive investigation into the photometric variation of red sequence modal galaxy colours with environment. The clusters span a range of Bautz-Morgan types and evolutionary stages and are shown to be representative of the global underlying intermediate L_X cluster sample. We define cluster membership using SDSS spectroscopic data and characterize the clusters by deriving new recession velocities, velocity dispersions and other parameters for each. We construct colour-magnitude diagrams for each of these clusters and obtain the position of the red sequence using a robust line fitting algorithm with a Lorentzian merit function. In doing so, we describe a population of discordant points on the colour-magnitude plane which are the result of photometric blending, dust and other causes. By fitting the clusters with Schechter functions to derive M^* values in each SDSS passband, we combine the red sequence of the galaxy clusters together to form a composite sample. We detail how the modal colour value of the red sequence varies with radius from the centre of this composite cluster and local galaxy density for all SDSS colours. In agreement with previous studies, these colours are shown to systematically move blueward with increasing distance from the cluster centres, or equivalently lower local galaxy density, whilst the width of the red sequence increases. This supports the idea that the galaxies at the outskirts of these clusters have younger luminosity-weighted ages than those at the core indicating their star formation has been quenched more recently than in the core. A comparison of our derived gradients in $(g - r)$ (explicitly: $d(g - r)/d\log(r_p) = -0.031 \pm 0.003$ and $d(g - r)/d\log(\Sigma) = 0.012 \pm 0.002$) with earlier works tentatively suggests that these gradients vary redshift which would reflect the hierarchical build-up of the red sequence over time.

Key words: galaxies: clusters: general — galaxies: evolution — galaxies: elliptical and lenticular, cD

1 INTRODUCTION

A lot of effort has been devoted to understanding how galaxies evolve in clusters over recent years. Most of the attention has been placed on the highest-mass clusters, largely because they are the easiest ones to detect to high-redshift, and therefore can be contrasted to lower redshift analogues (e.g. Yee et al. 1996; Balogh et al. 1999; Fasano et al. 2000; Ebeling et al. 2001; Fairley et al. 2002; Poggianti et al. 2004;

Wake et al. 2005; Pimbblet et al. 2006; Poggianti et al. 2009; Valentuzzi et al. 2011). With a few notable exceptions (e.g. Andreon et al. 2004; the WINGS survey of Fasano et al. 2006), intermediate and low-mass clusters ($L_X \sim 1 \times 10^{44}$ erg s⁻¹) are a relatively unexplored region of parameter space and thus merit attention.

Interpreting X-ray luminosity, L_X , as a proxy for cluster mass, the bias toward high mass is immediately apparent in a diagram of X-ray luminosity-redshift parameter space. In Fig. 1, we present the regions of this parameter space explored by four X-ray luminosity-selected galaxy cluster studies – the Las Campanas/Anglo-Australian Telescope

* email:pjensen@swin.edu.au

† email:kevin.pimbblet@monash.edu

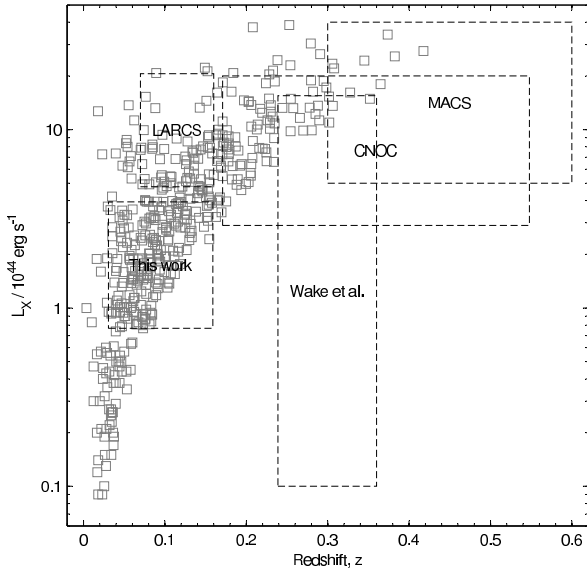


Figure 1. X-ray luminosity-redshift parameter space diagram. The grey squares represent XBACS, BCS, and eBCS clusters (Ebeling et al. 1996; 1998; 2000) while the dashed line boxes show the region of parameter space probed by a small variety X-ray selected cluster studies. Note that CNOC, MACS and Wake et al. select clusters from catalogues other than XBACS, BCS, and eBCS – only LARCS and this present study use the clusters contained inside the boxes displayed and we emphasize that all works concerned attempt to minimize Malmquist bias. The plot serves to demonstrate the bias to high L_X clusters being visible to high redshift and here we contend that we need a lower redshift, homogeneously selected baseline of intermediate- L_X clusters to compare these other works to.

Rich Cluster Survey (LARCS; Pimblet et al. 2001; 2002; 2006), the Canadian Network for Observational Cosmology (CNOC) Cluster Redshift Survey (Yee et al. 1996; Balogh et al. 1999), the Massive Cluster Survey (MACS; Ebeling et al. 2001) and the work of Wake et al. (2005) – as well as the region explored by this work.

Given that luminosity-selected cluster surveys can be subject to such a Malmquist bias, a number of observational strategies are possible. The MACS and CNOC studies opt for a high L_X , longitudinal redshift strategy whereas the LARCS study focused on creating a homogeneous sample at low-redshift. In contrast, Wake et al. probes a wide range of X-ray luminosities at intermediate redshift by selecting clusters from a variety of surveys with different flux limits. A drawback of selecting clusters from multiple sources though, is that unforeseen biases may be introduced into the sample. Furthermore, such works do not tell us much about intermediate-mass clusters; for example, Wake et al. (2005) only looks at 12 clusters of which only 4 are found within the L_X limits of this work – comparable arguments can be extended to other studies (e.g. Huertas-Company et al. 2009). To address this issue, we assemble a sample of intermediate L_X galaxy clusters with spectroscopically confirmed members from the Sloan Digital Sky Survey (SDSS Data Release 6, Adelman-McCarthy et al. 2008; see also York et al. 2000)

to examine the role of environment on the colour-magnitude relationship in such systems.

On the colour-magnitude plane, there are two distinct galaxy populations residing in galaxy clusters. The first population is mainly composed of early-type (E and S0) galaxies which form a tight, linear relation extending to the brightest magnitude galaxies on this plane. This population is known as the red sequence and the ridge line upon which the red sequence galaxies lie is known as the colour-magnitude relation (CMR; Visvanathan & Sandage 1977). Subsequent studies (e.g. Bower, Lucey & Ellis 1992) have demonstrated the universal existence of a red sequence in all clusters. At faint magnitudes, the red sequence is observed to fan out on the colour-magnitude plane (Kodama & Bower 2001; Pimblet et al. 2002). This effect has been interpreted in terms of the age-metallicity relation – the increasing spread of galaxy colours is the result of an increasing spread of galaxy metallicities and ages (Kodama et al. 1999; see also Kodama & Arimoto 1997). The second population is mainly composed of bluer, fainter-magnitude, morphologically spiral and star-forming galaxies which lie underneath the CMR – the so-called blue cloud (see, e.g., Poggianti et al. 2006, Cortese & Hughes 2009, Mei et al. 2009 and references therein). The evolution of this latter population in to the former has been extensively investigated in the literature (e.g. Kodama & Bower 2001; De Lucia et al. 2004; McIntosh et al. 2004; Tanaka et al. 2005; Tran et al. 2005; Haines et al. 2006; De Lucia et al. 2007; Stott et al. 2007; Ma et al. 2010; Jiménez et al. 2011) and relates to the origin of observed correlations such as the morphology-density relation (Dressler 1980) and related issues (cf. Lewis et al. 2002; Gómez et al. 2003; Butcher & Oemler 1984; see also Mahajan & Raychaudhury 2009). The developing picture is that as low mass, blue galaxies accrete on to the cluster potential, their star-formation is truncated (possibly after an intense starburst event; cf. Sato & Martin 2006) and their morphologies altered (by a variety of physically-motivated mechanisms) as they join more massive dark matter halos (e.g. Gunn & Gott 1972; Larson et al. 1980; Byrd & Valtonen 1990; Moore et al. 1996; Dressler et al. 1997; Quilis et al. 2000; Balogh et al. 2000; Diaferio et al. 2001; De Lucia et al. 2004).

In this context, a number of authors have presented evidence for an environmental¹ dependence of galaxy observables. For instance, Abraham et al. (1996) make use of a combined spectroscopic and photometric survey of Abell 2370 to show that radial gradients across the cluster exist out to a remarkably large radius (~ 5 Mpc). In particular, the colours of CMR galaxies are shown to become progressively bluer with projected radius (independent of mass) from the cluster centre which is mirrored by a change in Balmer line indices. The natural interpretation of these results is that the mean luminosity-weighted age of the stellar populations in the cluster galaxies is decreasing with increasing radius from the cluster centre as new galaxies and groups

¹ The word ‘environment’ has been taken to mean various things in the literature by different authors (see Haas, Schaye, & Jeon-Daniel 2011). This includes but is not limited to: radius from a cluster centre, local galaxy density, dark matter halo mass of a galaxy, and large-scale structural situation (e.g. void vs. filament vs. cluster).

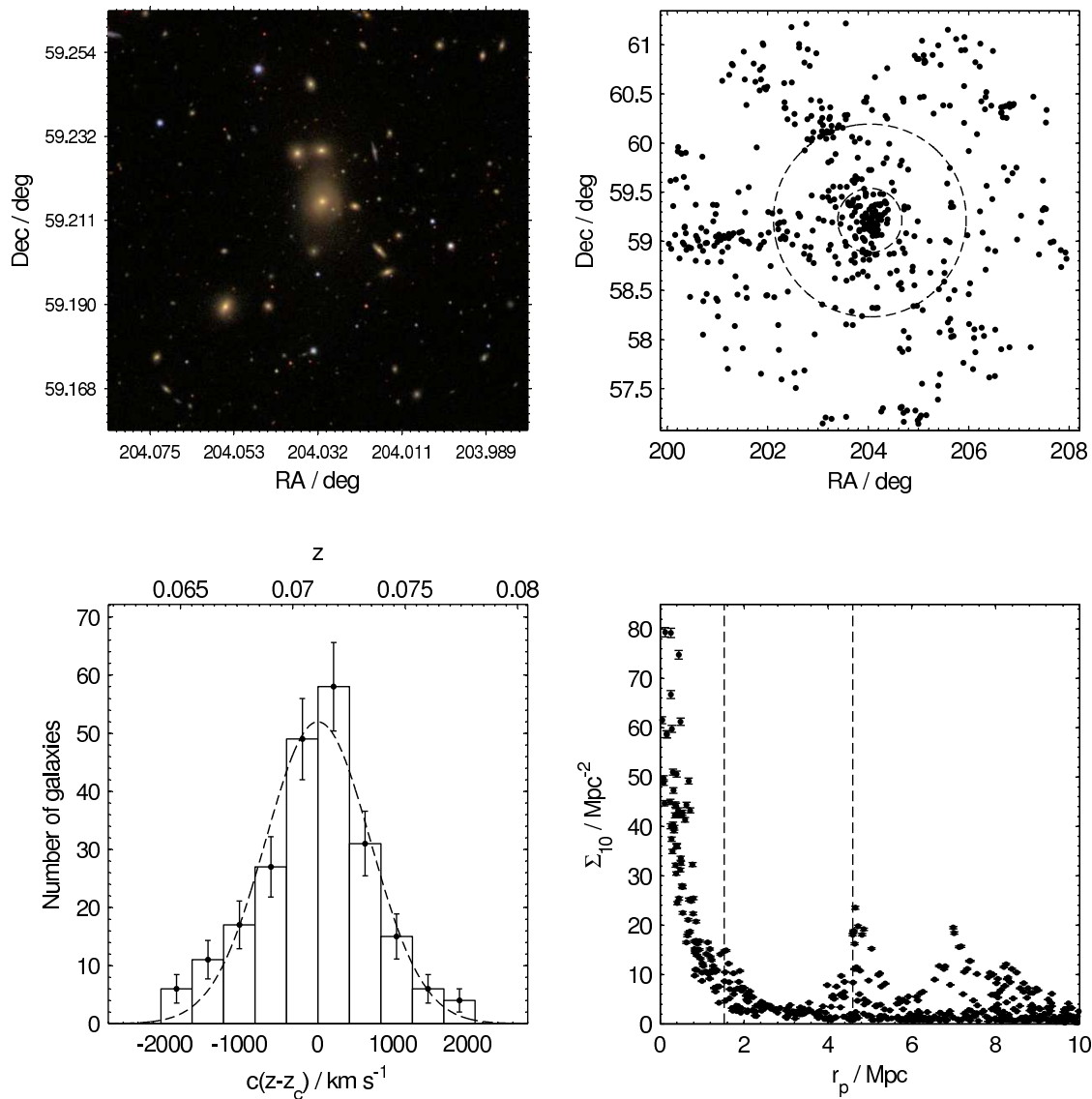


Figure 2. Diagnostic plots for Abell 1767 – a representative cluster from our sample. Top Left: SDSS image of the inner 0.5×0.5 Mpc of the cluster core. Top Right: RA and Dec of all galaxies within 10 Mpc of the cluster centre. The inner circle denotes r_{200} and the outer circle is $3r_{200}$. Bottom Left: Redshift histogram for the cluster with the fitted Gaussian overplotted that was used to determine the redshift and velocity dispersion of the cluster. Bottom Right: A diagnostic plot of local galaxy density (Σ_{10}) as a function of projected radius from the cluster centre. The two vertical lines correspond to radii of r_{200} and $3r_{200}$. Abell 1767 is a rich Bautz-Morgan type II cluster fed by multiple filaments of galaxies (cf. Pimblet et al. 2004) with some substructure – indicated by the peaks in Σ_{10} that are prominent at $3r_{200}$ and beyond.

are accreted from filaments, fuelling the cluster’s growth (see also Bernardi et al. 2006; Smith et al. 2006).

Other studies followed Abraham et al. (1996) and found similar results in other clusters (e.g. Terlevich et al. 2001 for the Coma cluster; Haines et al. 2004). Pimblet et al. (2002; 2006) generalized these results for a very X-ray luminous sample of $z \sim 0.1$ galaxy clusters: a gradient of $d(B-R)/dr_p = -0.022 \pm 0.004$ was found for CMR galaxies out to 6 Mpc suggesting that galaxies in the outer regions of the rich clusters have not yet had their star-formation

rates fully truncated. Concerned that such results may not be typical or representative of all clusters (since Pimblet et al. only examined the extrema of the cluster mass function), Wake et al. (2005) extend this study to lower X-ray luminosities at modest redshifts and found similar results (see their Fig. 13; see also Hogg et al. 2004). Yet, as noted above, this study only constituted a small number of clusters at intermediate L_X . Therefore in this work, we aim to generalize these results to intermediate L_X ranges through a purpose-constructed, representative sample of clusters.

The format of this work is as follows. In Section 2, we construct a sample of 45 intermediate L_X galaxy clusters at low redshift that are covered by SDSS data. We show that these are representative of the general cluster population for these luminosities and extract SDSS data for all member galaxies. In Section 3 we present Schechter function fits which we use to define a characteristic magnitude for stacking galaxy clusters. We also present the cluster colour-magnitude diagrams which are used to identify red sequence galaxies. In Section 4, we stack the clusters to form a composite sample from which we determine the photometric gradients of the red sequence galaxies in all SDSS colours. We describe how our results fit in with previous studies and suggest the existence of relationships of modal colour gradient with L_X and redshift. Our major results are then summarized in Section 5.

Throughout this work, we adopt the standard flat cosmology from Spergel et al. (2007): $\Omega_M = 0.24$, $\Omega_\Lambda = 0.76$ and $H_0 = 73 \text{ km s}^{-1} \text{ Mpc}^{-1}$.

2 DATA

Galaxy clusters are selected for this work from the X-ray Brightest Abell Cluster Survey (XBACS), the ROSAT Brightest Cluster Sample (BCS) and the ROSAT Extended Brightest Cluster Survey (eBCS) catalogues (Ebeling et al., 1996; 1998; 2000). Briefly, the XBACS, BCS and eBCS catalogues list many extended, extragalactic X-ray sources from ROSAT All-Sky Survey data. Clusters are detected in the soft X-ray band between 0.1–2.4 keV. In total, the catalogues contain 462 unique galaxy clusters of which 214 satisfy $0.7 \times 10^{44} < L_X < 4 \times 10^{44} \text{ ergs}^{-1}$ and $0.03 < z < 0.16$ – our definition of a local sample of intermediate L_X galaxy clusters.

We use SDSS DR6 (Adelman-McCarthy et al. 2008) as our photometric and spectroscopic catalogue in this work, which immediately cuts down the number of potential clusters available to study due to the spatial coverage of SDSS and also restricts our coverage to modestly bright magnitudes. The SDSS main sample spectroscopic target list contains all galaxies brighter than $r = 17.77$ (Strauss et al. 2002) but due to fibre collisions (cf. Blanton et al. 2003), the completeness level at $r = 17.77$ may be slightly lower than 100 per cent at this magnitude. In Fig. 3 we display our own estimate of the completeness of our catalogue and find that at $r = 17.77$, we are still ~ 95 per cent complete which should be more than sufficient for the present work.

Preliminary cluster membership is determined by extracting galaxies within $z \pm 0.02$ of the nominal cluster redshift given by XBACS, BCS and eBCS out to a projected radius of 10 Mpc from the cluster centre (defined as the X-ray luminosity peak of the cluster). For each cluster, we determine final membership by fitting a Gaussian to the redshift distribution of the preliminary members (Fig. 2). Using the position of the peak of the Gaussian as the updated cluster redshift, we proceed to eliminate any galaxies outside $3\sigma_z/c$ of the updated redshift (i.e. a sigma-clipping process; cf. Yahil & Vidal 1977). This process is iterated twice to produce the final membership for the clusters in our sample. Although we may miss real cluster members through this method (cf. section 4.2 of Pimblet et al. 2006), it will suf-

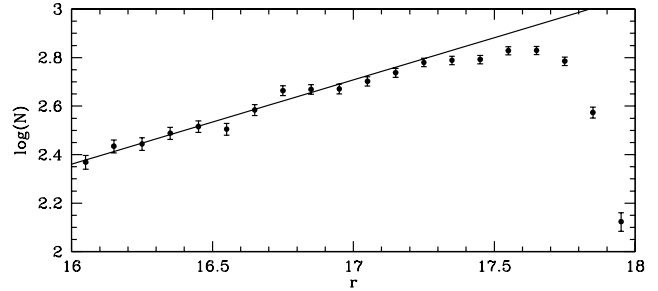


Figure 3. Histogram of r-band magnitudes for our galaxy sample. To determine how complete our sample is, we fit a line to the brighter part of this plot ($16 < r < 17$) where we are confident of being 100 per cent complete and extrapolate this to fainter magnitudes. At $r = 17.77$, our sample is still 95 per cent complete and we suggest that this level of completeness is sufficient for the present work.

fice for our purposes as we will later stack all of our clusters together to form a composite.

To ensure that this method is robust against choice of bin size in constructing the redshift histogram, Gaussian fit coefficients for the redshift histograms are estimated iteratively by performing χ^2 minimizations on the histogram data points. One hundred iterations are performed for each cluster with new random bin sizes on each iteration. The best fit Gaussian coefficients and their associated errors are calculated from the mean and standard deviation values of the coefficients over 100 iterations. By randomising the bin sizes, we ensure that our best fit Gaussians are independent of binning bias.

Our examination of the clusters generated by this method (e.g., Fig. 2) returns a mixture of usable and unusable clusters. Here, we consider ‘unusable’ to be clusters with fewer than 50 members (this is driven by a need to maintain a high completeness in each cluster so that we can fit a line to the colour-magnitude relation of an individual cluster and so that an individually rich cluster will not dominate in a stacked, composite sample), those located in the ‘whisker’ regions of SDSS DR6 (i.e. those contained in the long, narrow stripes of spectroscopically-sampled sky near the celestial equator where we cannot probe out to $3r_{200}$) and over-lapping clusters. For the former issue, this introduces a minor bias to our target selection: low redshift clusters are much more able to enter our sample than higher redshift clusters (clusters at $z < 0.1$ have 182 ± 48 extra members compared to $z > 0.1$) meaning that some of the advantage our sample has (Fig. 1) is removed. However, if we were to add in clusters with < 50 members, their contribution to the final, composite cluster would be fractional (one extra cluster with < 50 members would increase our sample size by $\ll 0.5$ per cent) and our final results would not be significantly affected.

We define overlapping clusters as clusters which have their 10 Mpc projected radius search areas overlap with the search areas of other clusters within our L_X range. Removing the overlapping clusters simplifies our analysis because it means that we do not have to worry about how to assign cluster membership to galaxies located in the overlap regions and cross-contamination (explicitly, an overlapping neighbour will manifest itself as a second red sequence in

Table 1. Intermediate L_X galaxy cluster sample used in this work.

Cluster	$[10^{44} L_{\text{erg/s}}]$	B-M Type	Redshift	$[\sigma_z]$ [km/s]	r_{200} [Mpc]	C	S
Abell 602	1.14	III	0.06195 ± 0.00006	1080 ± 40	2.39 ± 0.01	0.53	yes
Abell 671	0.90	II-III	0.04926 ± 0.00003	600 ± 10	1.34 ± 0.01	0.64	?
Abell 743	2.71	III	0.13610 ± 0.00030	500 ± 200	0.93 ± 0.08	0.34	no
Abell 744	0.77	II	0.07298 ± 0.00009	240 ± 40	0.53 ± 0.02	0.65	no
Abell 757	0.90	III	0.05108 ± 0.00003	390 ± 10	0.88 ± 0.01	0.42	no
Abell 763	2.34	II-III	0.08924 ± 0.00008	380 ± 50	0.81 ± 0.02	0.43	no
Abell 923	2.07	II	0.11700 ± 0.00005	420 ± 30	0.88 ± 0.01	0.40	no
Abell 957	0.78	I-II	0.04546 ± 0.00005	850 ± 30	1.91 ± 0.01	0.55	no
Abell 961	3.14	II-III	0.12700 ± 0.00010	690 ± 40	1.43 ± 0.01	0.45	no
Abell 971	1.44	II	0.09320 ± 0.00002	762 ± 9	1.63 ± 0.01	0.78	no
Abell 1035	0.92	II-III	0.06721 ± 0.00005	720 ± 30	1.59 ± 0.01	0.61	?
Abell 1045	3.47	II-III	0.13780 ± 0.00070	600 ± 100	1.28 ± 0.05	0.28	no
Abell 1126	1.15	I-II	0.08433 ± 0.00007	350 ± 50	0.75 ± 0.02	0.46	no
Abell 1361	3.59	I-II	0.11549 ± 0.00005	640 ± 20	1.33 ± 0.01	0.45	no
Abell 1446	1.30	II-III	0.10280 ± 0.00010	710 ± 60	1.51 ± 0.02	0.52	no
Abell 1691	0.89	II	0.07176 ± 0.00002	650 ± 8	1.42 ± 0.01	0.52	yes
Abell 1728	1.29	I-II*	0.08965 ± 0.00002	940 ± 10	2.02 ± 0.01	0.34	yes
Abell 1767	2.47	II	0.07112 ± 0.00002	700 ± 20	1.53 ± 0.01	0.54	?
Abell 1773	1.53	III	0.07727 ± 0.00003	790 ± 40	1.72 ± 0.01	0.53	yes
Abell 1809	1.61	II	0.07938 ± 0.00001	808 ± 7	1.76 ± 0.01	0.76	?
Abell 1814	2.82	II	0.12673 ± 0.00009	330 ± 50	0.68 ± 0.02	0.72	no
Abell 1831	1.90	III	0.06311 ± 0.00003	480 ± 10	1.06 ± 0.01	0.52	yes
Abell 1885	2.40	II-III	0.09200 ± 0.00200	1100 ± 500	2.40 ± 0.20	0.80	?
Abell 1925	1.56	II	0.10570 ± 0.00007	580 ± 30	1.22 ± 0.01	0.34	?
Abell 1927	2.14	I-II	0.09506 ± 0.00003	520 ± 20	1.12 ± 0.01	0.37	no
Abell 2033	2.57	III	0.07828 ± 0.00003	1049 ± 9	2.28 ± 0.01	0.51	yes
Abell 2108	1.97	III	0.09033 ± 0.00008	750 ± 30	1.60 ± 0.01	0.51	no
Abell 2110	3.93	I-II	0.09728 ± 0.00005	630 ± 40	1.35 ± 0.02	0.42	no
Abell 2124	1.35	I	0.06723 ± 0.00002	740 ± 10	1.62 ± 0.01	0.68	no
Abell 2141	3.89	II	0.15900 ± 0.00030	900 ± 300	1.80 ± 0.10	0.80	no
Abell 2148	1.39	III*	0.08843 ± 0.00005	570 ± 20	1.22 ± 0.01	0.57	?
Abell 2149	0.83	II-III*	0.06503 ± 0.00003	280 ± 20	0.61 ± 0.01	0.35	no
Abell 2175	2.93	II	0.09646 ± 0.00004	780 ± 10	1.65 ± 0.01	0.44	no
Abell 2199	3.70	I	0.03055 ± 0.00001	681 ± 1	1.56 ± 0.01	0.43	yes
Abell 2228	2.81	I-II	0.10102 ± 0.00004	980 ± 20	2.09 ± 0.01	0.41	no
RXJ0820.9+0751	2.09	I-II*	0.11032 ± 0.00007	560 ± 30	1.17 ± 0.01	0.54	no
RXJ1000.5+4409	3.08	III*	0.15310 ± 0.00030	700 ± 100	1.33 ± 0.05	0.82	?
RXJ1053.7+5450	1.04	III*	0.07291 ± 0.00004	580 ± 20	1.27 ± 0.01	0.62	yes
RXJ1423.9+4015	0.94	III*	0.08188 ± 0.00005	460 ± 10	0.99 ± 0.01	0.54	?
RXJ1442.2+2218	2.66	II*	0.09613 ± 0.00007	470 ± 70	1.01 ± 0.03	0.42	?
RXJ1652.6+4011	2.85	III*	0.14800 ± 0.00020	750 ± 90	1.52 ± 0.03	0.45	yes
ZwCl 1478	2.38	II-III*	0.10300 ± 0.00080	400 ± 200	0.82 ± 0.08	0.35	no
ZwCl 4905	1.20	I-II*	0.07641 ± 0.00003	480 ± 20	1.04 ± 0.01	0.48	no
ZwCl 6718	1.24	II*	0.07220 ± 0.00020	400 ± 200	0.85 ± 0.09	0.55	no
ZwCl 8197	2.89	II*	0.11320 ± 0.00010	830 ± 100	1.74 ± 0.04	0.31	no

a colour-magnitude diagram which will mean any fit to the colour-magnitude relation of an individual cluster is suspect at best). We caution that there may still be clusters overlapping with other clusters that are outside of our L_X range but we would anticipate that their influence on our result to be minimal when we later combine our clusters in to a composite sample.

Our final sample consists of 45 intermediate L_X galaxy clusters at a median redshift of $z = 0.0897$ which span a range of properties. For example, our richest cluster (Abell 2199) contains 1344 spectroscopically-confirmed members whereas our poorest cluster (Abell 1814) has 54 members.

We summarize our cluster sample and their global properties in Table 1.

To increase the utility of our analysis to other researchers (and our own future work), we derive several additional parameters for the clusters used in this work. Firstly, included in Table 1 are Bautz-Morgan classifications of our clusters (Bautz & Morgan 1970). Most of these are directly sourced from the NASA Extragalactic Database (NED), but those marked by an asterisk were manually determined by visual inspection by PCJ. Values for r_{200} are derived following Carlberg et al. (1997): $R_{\text{virial}} \approx r_{200} = \sqrt{(3)\sigma_z/10H(z)}$ where $H(z) = H_0^2(1+z)^2(1+\Omega_M z)^2$ and σ_z is the velocity dispersion of the cluster. The concentration indices (C)

are computed by sorting all galaxies within $3r_{200} \approx r_{100}$ in to projected radius order and applying $C = \log_{10}(r_{60}/r_{20})$ where r_{60} and r_{20} are the 20th and 60th percentiles of this distribution. We also make a qualitative judgment about whether the cluster has substructure (column headed S in Table 1) from inspection of a plot of local galaxy density² versus projected radius (Fig. 2). A peak outside of the cluster core in Σ_{10} is taken as a signature of substructure for this purpose. Although in principle we could have used other, quantitative methods (cf. Dressler & Shectman 1988; Ashman et al. 1994; see also Pimblet et al. 2011 and references therein) this approach is sufficient to make the statement that our sample has a range of clusters at a number of evolutionary stages. Including both clusters that have strong secondary Σ_{10} peaks and those with probable ones (i.e. both ‘yes’ and ‘?’ entries in the substructure column, S , of Table 1), our sample has 19 out of 45 clusters (~ 40 per cent) containing substructure. This is an under-estimate for intermediate L_X clusters overall since we have intentionally removed overlapping clusters to generate our sample (above) and we don’t search for line-of-sight substructure. We note that this value is intermediate to that predicted for rich clusters (e.g., Lacey & Cole 1993) and that observed in poor clusters (Burgett et al. 2004). This is in line with theoretical expectations that demonstrate intermediate- L_X clusters are expected to have accreted approximately 50 per cent of their total mass in the past ~ 7 Gyr (see Fig. 13 of Lacey & Cole 1993).

To characterize the dataset and address the question of whether our sample of 45 galaxy clusters is representative of the global intermediate L_X cluster population we compare the frequency of different Bautz-Morgan classifications in our sample and the parent XBACS, BCS and eBCS sample. This is graphically displayed in Fig. 4. In comparison to the full X-ray sample of intermediate L_X clusters, our cut-down sample appears to have a lower prevalence of BM I and slightly higher prevalence of BM II types. The fraction of BM III (and, indeed, intermediate BM types) appears to be similar in both populations. Despite this, the differences between the histograms are not significant at the 3σ level. We therefore contend that we have a representative sample of all intermediate L_X cluster types for this work. However, from Fig. 1 it is also apparent that we are not probing the lower right of the box denoting this work (i.e. clusters at the upper end of our redshift interval with low L_X). In acknowledging that this biases our cluster sample, we note the lookback time from the lowest redshift to the highest is some ~ 1.5 Gyr.

3 LUMINOSITY FUNCTION AND COLOUR-MAGNITUDE RELATIONS

Having defined our cluster sample and their galaxy members, we now create plots of colour-magnitude relationships for all of our clusters in a variety of broadbands (Fig. 5). In creating these colour-magnitude diagrams, we located a

² We define local galaxy density as Σ_{10} – the surface area on the sky that is occupied by a given galaxy and its 10 nearest neighbours. This measure of ‘environment’ probes the internal densities of the dark matter halos well (Muldrew et al. 2011).

Table 2. Values for M^* from fitting Schechter functions to the cluster galaxies.

Band	M^*
<i>u</i>	-18.29 ± 0.04
<i>g</i>	-20.35 ± 0.05
<i>r</i>	-21.09 ± 0.05
<i>i</i>	-21.53 ± 0.04
<i>z</i>	-21.81 ± 0.04

number of discordant points – galaxies that lie very far away from the bulk of the population. These galaxies are explored in detail in Appendix A but here we simply note that they are removed from the subsequent analysis as they may adversely affect the fit of the CMRs.

We first fit the absolute (k-corrected) magnitudes of the galaxy cluster members with a Schechter function (Schechter 1976) to determine M^* (a more physically meaningful parameter than absolute magnitudes) and therefore provide a pivot point which we will use to combine our CMRs together in to a stacked cluster (dashed vertical lines in Fig. 5). The k-corrections used in this work are from the PHOTOZ table of SDSS DR6 (<http://cas.sdss.org/astro/en/help/browser/browser.asp?n=Photoz%20&t=U>). Although these use photometric redshifts, the redshift contribution to the total error is insignificant in comparison to the error budget of the flux density which is rarely known to better than a few per cent (Hogg et al. 2002). For each absolute magnitude band, the Schechter functions are fit from the brightest magnitude bin up to the 90 per cent completeness limit (solid vertical line in Fig. 5; see Fig. 3 for the definition). One hundred χ^2 minimizations are performed with M^* , N^* and α as free parameters and with randomised bin sizes between 0.05 and 0.5 mag. The fit parameters for M^* and their associated errors were calculated as being the mean and standard deviation of the 100 runs. These values for M^* (critical to this study) are shown in Table 2. We note that single Schechter function fits are inadequate descriptions of the luminosity function at both the bright end (where double or Gaussian functions may be more appropriate; e.g. Thompson & Gregory 1993; Dahlé et al. 2004) and the faint end (since we truncate our fits to the 90 per cent completeness limit). They do, however, provide an excellent fit to the ‘knee’ of the distribution and consequentially M^* which is important to us as a pivot point since it does not significantly vary with redshift (Mobasher et al. 2003 and references therein). The values of M^* that we present in Table 2 are similar to other values reported for generic SDSS cluster populations (Popesso et al. 2005), but we refrain from a more detailed comparison of these luminosity functions since our cluster sample is constructed in a very different manner to those studies and with different goals in mind.

To fit the CMRs, we only use galaxies brighter than the 90 per cent completeness fiducial magnitudes (vertical solid line in Fig. 5). Since there are two overlapping galaxy populations on the colour-magnitude plane (red sequence and blue cloud), ordinary least squares fitting techniques are inadequate to fit the CMRs. Typically, ordinary least squares

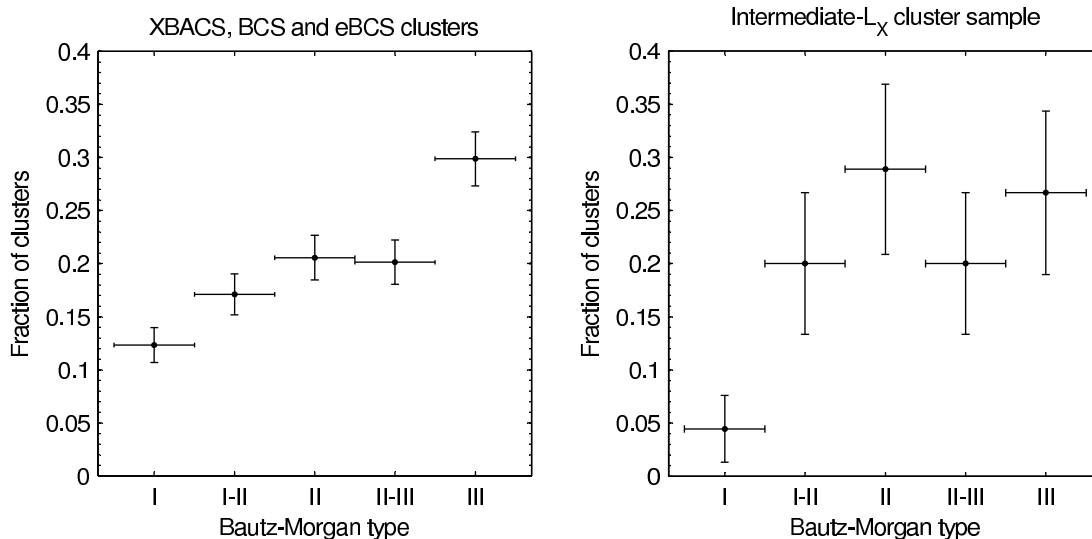


Figure 4. Bautz-Morgan fractions for the XBACS, BCS, and eBCS catalogues (462 clusters) and our cut-down intermediate L_X cluster sample (45 clusters). The vertical error bars are Poissonian. The two samples are not significant different at a 3σ level.

fitting yields slopes which are too steep and intercepts which are too high – the faint end of the CMR being dragged blueward by the blue cloud. Ideally, one would like to remove the blue cloud galaxies and perform an ordinary least squares fit to the remaining red sequence galaxies. However, identifying blue cloud galaxies without already knowing the position of the CMR is a non-trivial exercise. A more straightforward approach is to perform a robust linear fit which effectively weights red sequence galaxies higher than blue cloud galaxies (see for example Pimblet et al. 2002 who use a merit function which minimizes the sum of the absolute values of the residuals). Here, we follow a suggestion by Press et al. (1992) and use the Lorentzian merit function:

$$\sum_i \frac{\log(1 + r_i^2/2)}{\Delta y_i} \quad (1)$$

where Δy_i is magnitude of the error in y . In comparison to the absolute deviation minimizing merit function, the Lorentzian merit function visually appears to converge at least as well or closer to the apparent red sequence. The merit function was minimized using the Nelder-Mead downhill simplex algorithm (Press et al. 1992). The Nelder-Mead algorithm requires initial guess values for the linear fit coefficients – we use ordinary least squares regression fit coefficients as our starting points.

In almost all cases our approach successfully located the CMR in each diagram. However, the algorithm failed for a few clusters. In these cases, we impose a colour envelope around the (eyeball determined) location of the CMR to help the algorithm hone in on the CMR on a second run. All fits are double-checked by eye to confirm the approach works (Fig. 5).

4 COMPOSITE CLUSTER AND DISCUSSION

We now exploit the homogeneity of our sample and stack our clusters together to form a composite. This is achieved by applying colour and magnitude transformations to the CMRs of each of our clusters (Fig. 5) in a two-step process. Firstly, we remove the slope of the CMR and secondly, we evolve the individual clusters to a common redshift.

For each cluster we identify a pivot point which we define to be the intersection of the CMR with M^* . We rotate every point on the colour-magnitude diagram about this pivot point such that the CMR becomes horizontal. We emphasize that the slopes of the CMRs of the individual clusters have been found in an homogenous manner for our sample – an absolute requirement given the uncertainties (cf. Pimblet et al. 2002).

We then evolve the clusters to our mean redshift ($z = 0.0897$) by performing a vertical colour shift and an horizontal magnitude shift. The colour scale of each cluster is shifted so that the red sequence ridge lines are stacked on top of each other at a colour consistent with M^* at the mean redshift of the sample. The magnitude scale of each cluster is also shifted so that the M^* value of each cluster coincides. Fig. 6 displays the colour-magnitude diagram of the composite cluster in (g-i) versus i . Analogous plots are created for the other colour versus magnitude combinations permitted by the SDSS data.

We now turn to the environmental dependence of the modal colour of the CMR. We define modal colour to be the colour corresponding to the peak of a Gaussian fitted to the CMR peak of colour histogram of the composite cluster. To probe modal colour dependence as a function of cluster environment, we employ a method similar to the one described in Pimblet et al. (2002; 2006). Briefly, this is done by dividing the composite CMR (Fig. 6) into projected radius (via a fixed metric) and local galaxy density bins down to a fixed absolute magnitude limit ($M^* + 1$). Although we could have chosen r_{200} to place our clusters on to a more

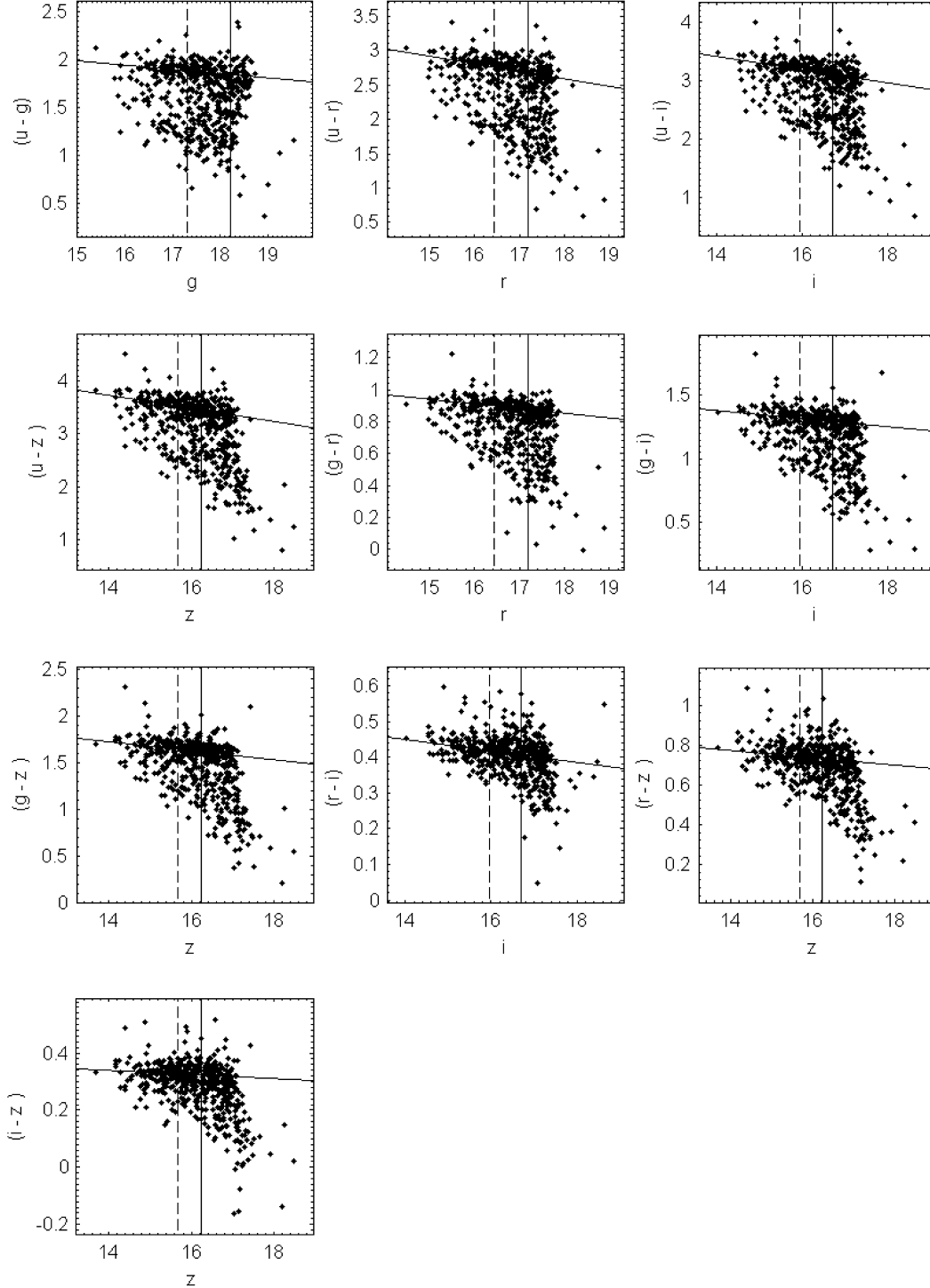


Figure 5. Colour-magnitude diagrams for Abell 1767 in a variety of broadbands for all member galaxies within 10 Mpc of the cluster centre (see Fig. 2). For each diagram, we fit the red sequence (diagonal solid line) as described in the text. The vertical lines denote M^* (dashed line) and our fiducial magnitude (solid line) which represents a 90 per cent completeness limit for our sample (see Fig. 3). We use M^* as the point about which we pivot the plots to create the composite cluster. Analogous diagrams are constructed for the other clusters in our sample.

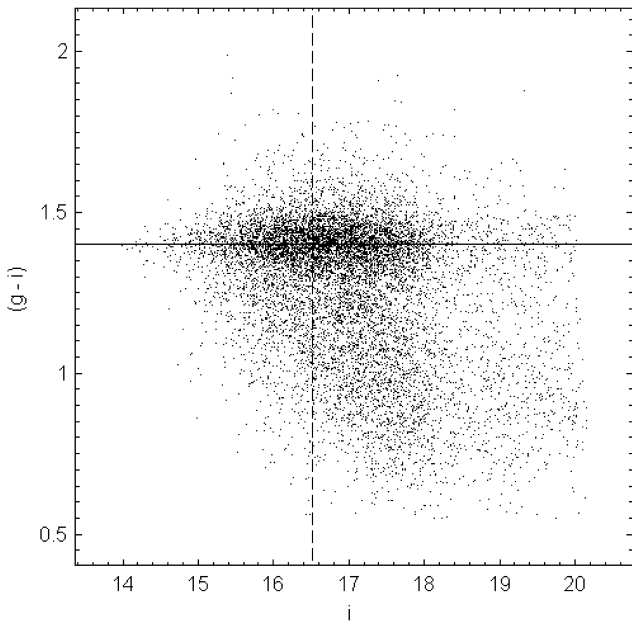


Figure 6. Composite $z \sim 0.09$ cluster colour-magnitude diagram in $(g-i)$ versus i for all 45 clusters in our sample. The solid horizontal line denotes the transformed position of the CMR of all the individual clusters whilst the vertical dashed line is M^* .

physically-motivated spatial scale, we choose to use a fixed metric since $r_{200} \approx r_{\text{virial}}$ has only a weak dependence on X-ray luminosity (Babul et al. 2002; see also Pimblet et al. 2002). Given the narrow L_X range of our sample, the variation of r_{200} for the cluster sample is predicted to be small (indeed, this prediction is borne out in our calculations presented in Table 1) hence the clusters are scaled to the fixed metric for simplicity.

In Fig. 7 we present the dependence of the modal CMR value on these two parameters. Qualitatively in-line with previous works (Abraham et al. 1996; Terlevich et al. 2001; Pimblet et al. 2002; Wake et al. 2005; Pimblet et al. 2006; see also Girardi et al. 2003; Haines et al. 2004), we observe the modal red sequence colour become progressively bluer with radius away from the cluster centre and, equivalently, decreasing local galaxy density. At the same time, the width of the red sequence is observed to increase. Similar results are obtained for the other SDSS bands. The strongest gradient in modal colour occurs for the inner portions (equivalently, high density regions) of these plots (see Fig. 7). We interpret the increasing width and bluening of the CMR as an age-metallicity effect (Kodama & Arimoto 1997; Kodama & Bower 2001; Pimblet et al. 2006) whereby the red sequence galaxies on the outskirts of the clusters have younger luminosity-weighted ages than those at the core. One potential issue with the increasing width is that as one moves from the cluster core to its outskirts, the mixture of the galaxies may be changing. For instance, the typical galaxy at higher radius may have a lower mass. This would result in larger error bars on the colour of the galaxy and could naturally explain the increase in width as simply being a relic of measurement errors. The colour error budget is, however, dominated by the fainter galaxies at all radii (simply due to their

Table 3. Modal colour gradient for the various SDSS colours as a function of projected radius and local galaxy density.

Radial Gradient	Value
$d(u-g)/d\log(r_p)$	-0.069 ± 0.007
$d(u-r)/d\log(r_p)$	-0.099 ± 0.008
$d(u-i)/d\log(r_p)$	-0.130 ± 0.020
$d(u-z)/d\log(r_p)$	-0.130 ± 0.010
$d(g-r)/d\log(r_p)$	-0.031 ± 0.003
$d(g-i)/d\log(r_p)$	-0.049 ± 0.004
$d(g-z)/d\log(r_p)$	-0.073 ± 0.006
$d(r-i)/d\log(r_p)$	-0.018 ± 0.002
$d(r-z)/d\log(r_p)$	-0.035 ± 0.004
$d(i-z)/d\log(r_p)$	-0.015 ± 0.002
Density Gradient	Value
$d(u-g)/d\log(\Sigma)$	0.025 ± 0.004
$d(u-r)/d\log(\Sigma)$	0.041 ± 0.004
$d(u-i)/d\log(\Sigma)$	0.043 ± 0.006
$d(u-z)/d\log(\Sigma)$	0.048 ± 0.007
$d(g-r)/d\log(\Sigma)$	0.012 ± 0.002
$d(g-i)/d\log(\Sigma)$	0.020 ± 0.003
$d(g-z)/d\log(\Sigma)$	0.024 ± 0.005
$d(r-i)/d\log(\Sigma)$	0.007 ± 0.001
$d(r-z)/d\log(\Sigma)$	0.017 ± 0.002
$d(i-z)/d\log(\Sigma)$	0.009 ± 0.001

numbers). The median $(g-r)$ colour error in our composite cluster at < 1 Mpc is 0.009, which increases to 0.010 at 5–6 Mpc. These figures \sim halve if we consider only galaxies with $M_r < -21$ and increase by some ≈ 0.005 for $M_r > -20$ galaxies. In all cases, the change in the photometric error with radius from the cluster centre is much less than the CMR width (Fig. 7) and at most contributes a quarter of the CMR’s width (i.e. at low radii). We also check the reality of the radial bluening by isolating samples in different absolute magnitude ranges (i.e. a mass proxy). In all cases, a bluerward trend of modal CMR colours is found.

In Table 3 we give the colour gradient for the inner regions of the composite cluster to the limit where the gradient becomes zero for all of the SDSS colours. This is the most comprehensive reporting of modal colour variations across clusters to date that we are aware of. Hence to compare this with other studies, we must restrict ourselves to more commonly used colours – e.g. our reported $(g-r)$ colour gradient. In Fig. 8 we display the radial $(g-r)$ gradient with the results reported by Abraham et al. (1996), Terlevich et al. (2001), Pimblet et al. (2002), and Wake et al. (2005)³ together with the gradient as a function of mean L_X for each of those studies.

There appears to be no correlation of X-ray luminosity – and therefore cluster mass by implication – for the radial colour gradients. However, Abraham et al. (1996) and Terlevich et al. (2001) are only single-case studies (Abell 2370 and Coma respectively). Therefore the gradients reported in those works may reflect the individual accretion history of those clusters rather than the more general results presented

³ We transform the colours reported in these studies to $(g-r)$ colours through the transforms presented by Smith et al. (2002).

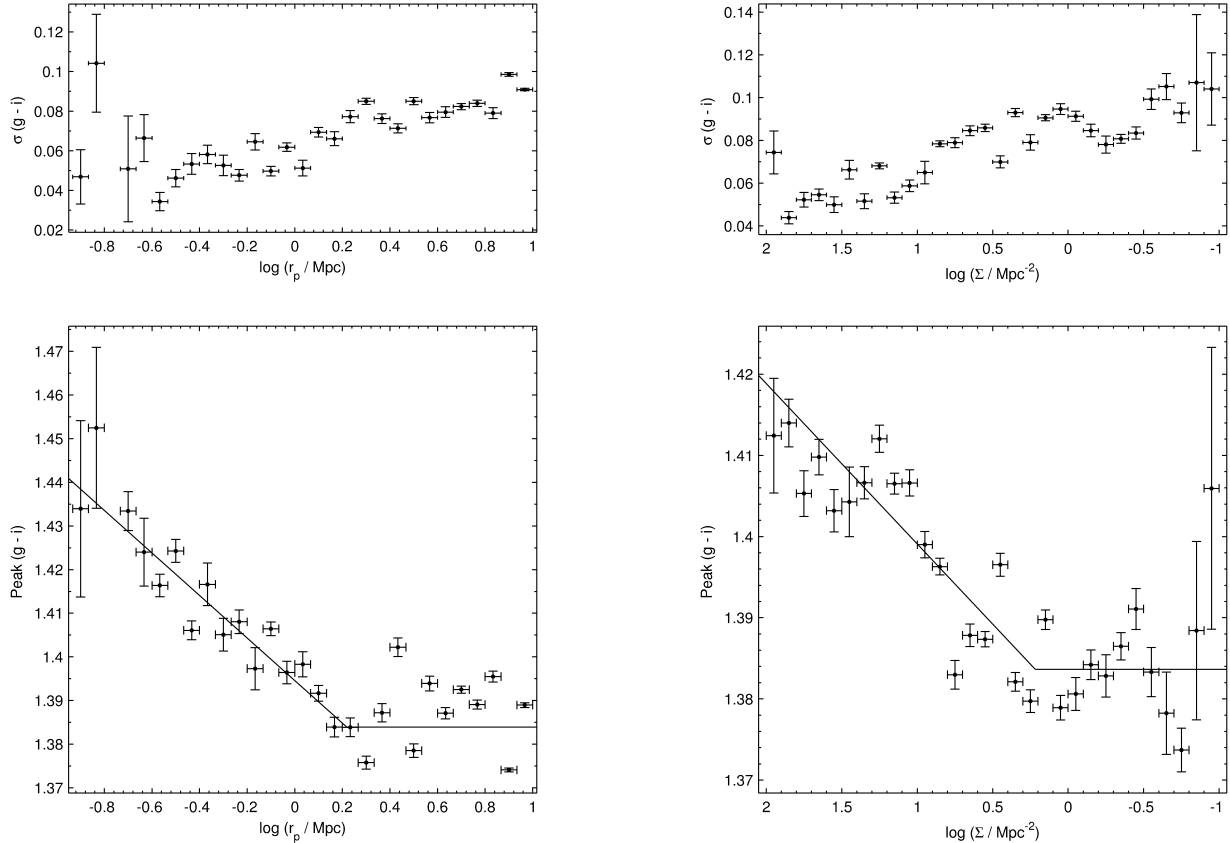


Figure 7. Environmental dependence of the width (upper panels) and modal value of the red sequence peak (lower panels). The colours of the CMR galaxies become progressively bluer with increasing radius from the cluster centre and decreasing local galaxy density (the lines in the lower panels are two linear fits to the points, divided where the gradient becomes approximately zero). This is accompanied with an increase in the width of the CMR.

here and by Pimblet et al. (2002) and Wake et al. (2005). This is supported by the results of Stott et al. (2009) who find the CMR slope of Coma is very unusual compared to other clusters. Moreover, the range of L_X probed by Wake et al. (2005) means that that point should also be regarded as tentative. For our study and Pimblet et al. (2002), the cluster samples are intentionally limited in L_X and we therefore hypothesize that there may yet be a relationship between colour gradient and L_X such that the gradient becomes steeper with increasing L_X values. A targeted study of a carefully constructed sample of low L_X clusters is therefore urgently needed to attempt to falsify this hypothesis.

Applying the same logic to the redshift evolution, we contend that the radial variation of the modal CMR colour gets increasingly strong at higher redshift. That said, we are not necessarily comparing like clusters with each other over that redshift range – the progenitors of our sample are most certainly not going to be higher L_X clusters at higher redshifts. Given the median difference in L_X from our sample to (e.g.) LARCS, we estimate that the difference in total mass would be a factor of ~ 2 – 3 (Popesso et al. 2005; see also Stott et al. 2009). Since we do not expect significant

variation in these cluster’s luminosity functions over such a mass range (cf. De Propris et al. 1999), we would expect that any variation in cluster properties are reflective of evolutionary change over the redshift range. Further, we note that the range of L_X probed by Wake et al. (2005) does include some clusters in our own L_X interval, which adds weight to the above argument for redshift evolution. This trend would also be straight-forward to interpret: the red cores of clusters establish themselves at early times and gain mass through accreting bluer ‘field’ galaxies which progressively redden over time (cf. De Lucia et al. 2007; Kodama & Bower 2001; Martínez, Coenda & Muriel 2010). The colour gradient therefore becomes shallower as the blue galaxies transform to redder galaxies at higher radii from cluster centres at a fixed mass and reflects the hierarchical build-up of the red sequence over time.

5 SUMMARY

In this work, we have assembled a sample of intermediate X-ray luminosity galaxy clusters from SDSS photometry and

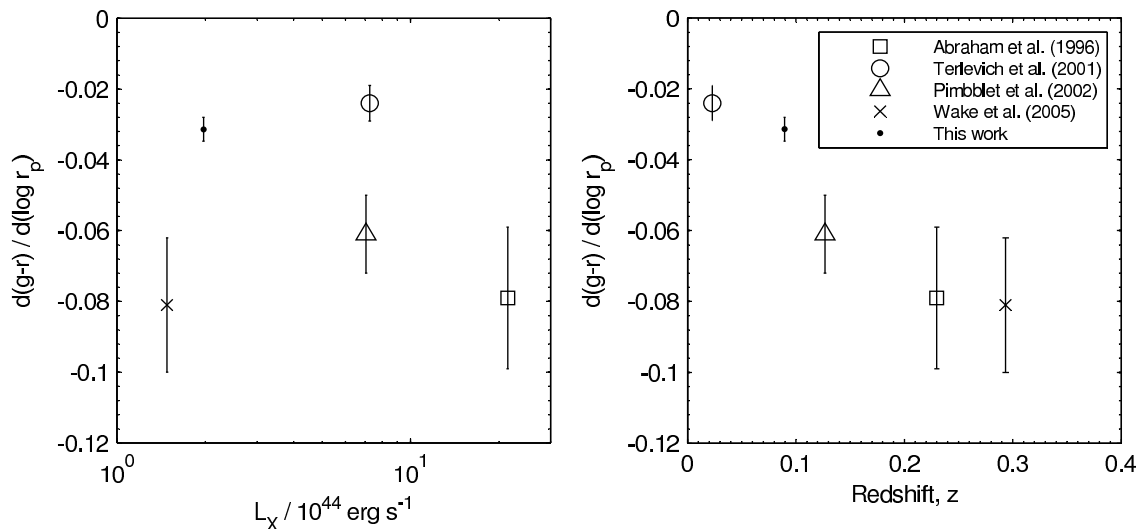


Figure 8. Comparison of reported $(g-r)$ CMR gradients from other X-ray selected cluster surveys with the present work. No trend is apparent with mean L_X (left), but this may reflect the nature of the individual clusters in each sample. Conversely, these works strongly suggest a steeper radial modal colour gradient with redshift (right).

spectroscopy. Our principal results are as follows:

- Strong colour-magnitude red sequences exist for our L_X range in all SDSS colours probed. As with higher L_X studies, these CMRs can be accessed to a large radius from the cluster centres, out in to the surrounding filamentary regime.
- The clusters exhibit a modal colour gradient for the red sequence galaxies in projected radius and local galaxy density whereby red sequence galaxies at the cluster outskirts are systematically bluer than those in the core for all SDSS colours. These gradients are interpreted as the galaxies at the cluster outskirts having younger luminosity-weighted ages.
- Our results agree with earlier measurements of colour gradients and extend them to comprehensively cover optical and near infra-red colours. They suggest that there may be a relationship between redshift and CMR colour gradient, but further studies using carefully constructed cluster samples are needed to verify this hypothesis and any potential relationship between L_X and colour gradient.

ACKNOWLEDGEMENTS

PCJ and KAP contributed equally to this manuscript.

PCJ acknowledges receipt of an Australian Postgraduate Award. KAP acknowledges partial support from the Australian Research Council and a Monash University internal grant scheme.

We thank Warrick Couch and Michael Drinkwater for helpful feedback on the content of this paper which is derived from PCJ's Honours Thesis, awarded by U. Queensland. Further, we gratefully thank the Astronomical Society of Australia for the award of the Bok Prize (2009) to PCJ for said thesis.

We also thank the anonymous referee for her/his constructive comments that have improved the work reported here.

Funding for the SDSS and SDSS-II has been provided by the Alfred P. Sloan Foundation, the Participating Institutions, the National Science Foundation, the U.S. Department of Energy, the National Aeronautics and Space Administration, the Japanese Monbukagakusho, the Max Planck Society, and the Higher Education Funding Council for England. The SDSS Web Site is <http://www.sdss.org/>.

The SDSS is managed by the Astrophysical Research Consortium for the Participating Institutions. The Participating Institutions are the American Museum of Natural History, Astrophysical Institute Potsdam, University of Basel, University of Cambridge, Case Western Reserve University, University of Chicago, Drexel University, Fermilab, the Institute for Advanced Study, the Japan Participation Group, Johns Hopkins University, the Joint Institute for Nuclear Astrophysics, the Kavli Institute for Particle Astrophysics and Cosmology, the Korean Scientist Group, the Chinese Academy of Sciences (LAMOST), Los Alamos National Laboratory, the Max-Planck-Institute for Astronomy (MPIA), the Max-Planck-Institute for Astrophysics (MPA), New Mexico State University, Ohio State University, University of Pittsburgh, University of Portsmouth, Princeton University, the United States Naval Observatory, and the University of Washington.

This research has made use of the NASA/IPAC Extragalactic Database (NED) which is operated by the Jet Propulsion Laboratory, California Institute of Technology, under contract with the National Aeronautics and Space Administration.

REFERENCES

Abraham R. G., et al., 1996, *ApJ*, 471, 694

- Adelman-McCarthy J. K., et al., 2008, *ApJS*, 175, 297
- Andreon S., Willis J., Quintana H., Valtchanov I., Pierre M., Pacaud F., 2004, *MNRAS*, 353, 353
- Ashman, K. M., Bird, C. M., & Zepf, S. E., 1994, *AJ*, 108, 2348
- Babul A., Balogh M. L., Lewis G. F., Poole G. B., 2002, *MNRAS*, 330, 329
- Balogh M. L., Morris S. L., Yee H. K. C., Carlberg R. G., Ellingson E., 1999, *ApJ*, 527, 54
- Balogh M. L., Navarro J. F., Morris S. L., 2000, *ApJ*, 540, 113
- Bautz L. P., Morgan W. W., 1970, *ApJ*, 162, L149
- Bernardi M., Nichol R. C., Sheth R. K., Miller C. J., Brinkmann J., 2006, *AJ*, 131, 1288
- Blanton M. R., Lin H., Lupton R. H., Maley F. M., Young N., Zehavi I., Loveday J., 2003, *AJ*, 125, 2276
- Bower R. G., Lucey J. R., Ellis R. S., 1992, *MNRAS*, 254, 589
- Burgett W. S., et al., 2004, *MNRAS*, 352, 605
- Butcher H., Oemler A., Jr., 1984, *ApJ*, 285, 426
- Byrd G., Valtonen M., 1990, *ApJ*, 350, 89
- Carlberg R. G., Yee H. K. C., Ellingson E., 1997, *ApJ*, 478, 462
- Cortese L., Hughes T. M., 2009, *MNRAS*, 400, 1225
- Dahlén T., Fransson C., Östlin G., Näslund M., 2004, *MNRAS*, 350, 253
- De Lucia G., et al., 2004, *ApJ*, 610, L77
- De Lucia G., et al., 2007, *MNRAS*, 374, 809
- Diaferio A., Kauffmann G., Balogh M. L., White S. D. M., Schade D., Ellingson E., 2001, *MNRAS*, 323, 999
- Dressler A., 1980, *ApJ*, 236, 351
- Dressler, A., & Shectman, S. A., 1988, *AJ* 95, 985
- Dressler A., et al., 1997, *ApJ*, 490, 577
- Ebeling H., Voges W., Bohringer H., Edge A. C., Huchra J. P., Briel U. G., 1996, *MNRAS*, 281, 799
- Ebeling H., Edge A. C., Bohringer H., Allen S. W., Crawford C. S., Fabian A. C., Voges W., Huchra J. P., 1998, *MNRAS*, 301, 881
- Ebeling H., Edge A. C., Allen S. W., Crawford C. S., Fabian A. C., Huchra J. P., 2000, *MNRAS*, 318, 333
- Ebeling H., Edge A. C., Henry J. P., 2001, *ApJ*, 553, 668
- Fairley B. W., Jones L. R., Wake D. A., Collins C. A., Burke D. J., Nichol R. C., Romer A. K., 2002, *MNRAS*, 330, 755
- Fasano G., Poggianti B. M., Couch W. J., Bettoni D., Kjærgaard P., Moles M., 2000, *ApJ*, 542, 673
- Fasano G., et al., 2006, *A&A*, 445, 805
- Girardi M., Mardirossian F., Marinoni C., Mezzetti M., Rigoni E., 2003, *A&A*, 410, 461
- Gómez P. L., et al., 2003, *ApJ*, 584, 210
- Gunn J. E., Gott J. R., III, 1972, *ApJ*, 176, 1
- Haas M. R., Schaye J., Jeeson-Daniel A., 2011, *MNRAS*, 1812
- Haines C. P., Mercurio A., Merluzzi P., La Barbera F., Massarotti M., Busarello G., Girardi M., 2004, *A&A*, 425, 783
- Haines C. P., Merluzzi P., Mercurio A., Gargiulo A., Krusanova N., Busarello G., La Barbera F., Capaccioli M., 2006, *MNRAS*, 371, 55
- Hogg D. W., Baldry I. K., Blanton M. R., Eisenstein D. J., 2002, *arXiv:astro-ph/0210394*
- Hogg D. W., et al., 2004, *ApJ*, 601, L29
- Huertas-Company M., Foex G., Soucail G., Pelló R., 2009, *A&A*, 505, 83
- Jiménez N., Cora S. A., Bassino L. P., Tecce T. E., Smith Castelli A. V., 2011, *MNRAS*, 417, 785
- Kodama T., Arimoto N., 1997, *A&A*, 320, 41
- Kodama T., Bower R. G., Bell E. F., 1999, *MNRAS*, 306, 561
- Kodama T., Bower R. G., 2001, *MNRAS*, 321, 18
- Lacey C., Cole S., 1993, *MNRAS*, 262, 627
- Larson R. B., Tinsley B. M., Caldwell C. N., 1980, *ApJ*, 237, 692
- Lewis I., et al., 2002, *MNRAS*, 334, 673
- Ma C.-J., Ebeling H., Marshall P., Schrabback T., 2010, *MNRAS*, 406, 121
- Mahajan S., Raychaudhury S., 2009, *MNRAS*, 400, 687
- Martínez H. J., Coenda V., Muriel H., 2010, *MNRAS*, 403, 748
- McIntosh D. H., Rix H.-W., Caldwell N., 2004, *ApJ*, 610, 161
- Mei S., et al., 2009, *ApJ*, 690, 42
- Mobasher B., et al., 2003, *ApJ*, 587, 605
- Moore B., Katz N., Lake G., Dressler A., Oemler A., 1996, *Natur*, 379, 613
- Muldrew S. I., et al., 2011, *MNRAS*, in press
- Pimblet K. A., Drinkwater M. J., Hawkrigg M. C., 2004, *MNRAS*, 354, L61
- Pimblet K. A., Smail I., Edge A. C., Couch W. J., O'Hely E., Zabludoff A. I., 2001, *MNRAS*, 327, 588
- Pimblet K. A., Smail I., Kodama T., Couch W. J., Edge A. C., Zabludoff A. I., O'Hely E., 2002, *MNRAS*, 331, 333
- Pimblet K. A., Smail I., Edge A. C., O'Hely E., Couch W. J., Zabludoff A. I., 2006, *MNRAS*, 366, 645
- Pimblet K. A., Andernach H., Fishlock C. K., Roseboom I. G., Owers M. S., 2011, *MNRAS*, 410, 1837
- Poggianti B. M., Bridges T. J., Komiyama Y., Yagi M., Carter D., Mobasher B., Okamura S., Kashikawa N., 2004, *ApJ*, 601, 197
- Poggianti B. M., et al., 2009, *ApJ*, 697, L137
- Popesso P., Böhringer H., Romaniello M., Voges W., 2005, *A&A*, 433, 415
- Press W. H., Teukolsky S. A., Vetterling W. T., Flannery B. P., 1992, *Numerical Recipes*, Cambridge University Press, Cambridge
- Quilis V., Moore B., Bower R., 2000, *Sci*, 288, 1617
- Sato T., Martin C. L., 2006, *ApJ*, 647, 946
- Schechter P., 1976, *ApJ*, 203, 297
- Smith J. A., et al., 2002, *AJ*, 123, 2121
- Smith R. J., Hudson M. J., Lucey J. R., Nelan J. E., Wegner G. A., 2006, *MNRAS*, 369, 1419
- Spergel D. N., et al., 2007, *ApJS*, 170, 377
- Stott J. P., Smail I., Edge A. C., Ebeling H., Smith G. P., Kneib J.-P., Pimblet K. A., 2007, *ApJ*, 661, 95
- Stott J. P., Pimblet K. A., Edge A. C., Smith G. P., Wardlow J. L., 2009, *MNRAS*, 394, 2098
- Strauss M. A., et al., 2002, *AJ*, 124, 1810
- Tanaka M., Kodama T., Arimoto N., Okamura S., Umetsu K., Shimasaku K., Tanaka I., Yamada T., 2005, *MNRAS*, 362, 268
- Terlevich A. I., Caldwell N., Bower R. G., 2001, *MNRAS*, 326, 1547
- Thompson L. A., Gregory S. A., 1993, *AJ*, 106, 2197
- Tran K.-V. H., van Dokkum P., Illingworth G. D., Kelson D., Gonzalez A., Franx M., 2005, *ApJ*, 619, 134
- Valentinuzzi T., et al., 2011, *A&A*, 536, A34
- Visvanathan N., Sandage A., 1977, *ApJ*, 216, 214
- Wake D. A., Collins C. A., Nichol R. C., Jones L. R., Burke D. J., 2005, *ApJ*, 627, 186
- Yahil A., Vidal N. V., 1977, *ApJ*, 214, 347
- Yee H. K. C., Ellingson E., Carlberg R. G., 1996, *ApJS*, 102, 269
- York D. G., et al., 2000, *AJ*, 120, 1579

APPENDIX A: DISCORDANT POINTS ON THE COLOUR-MAGNITUDE PLANES

In creating the colour-magnitude diagrams for our cluster sample (Fig. 5), we located a number of discordant galaxies whose position on the colour-magnitude plane was very much away from the bulk of the population (i.e. much redder than the red sequence or much bluer than the blue cloud).

The majority of the discordant points appear to be caused by photometric saturation from other objects nearby to the target galaxy. The most common source of colour bias

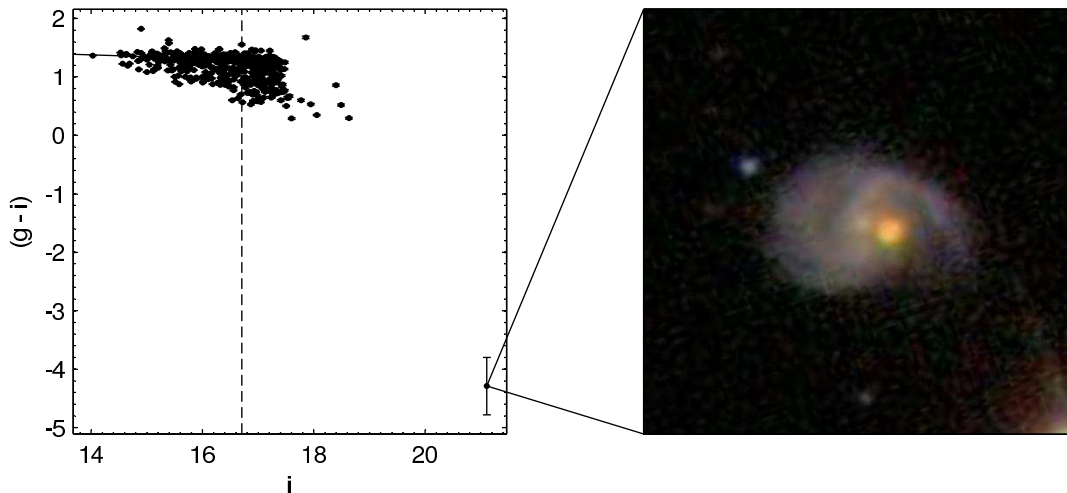


Figure 9. Discordant point on the $(g-i)$ versus i colour-magnitude diagram for Abell 1767. A blue spiral galaxy in the line-of-sight of the target red elliptical galaxy confuses the photometric measurements, causing the i band to be much fainter than the other bands.

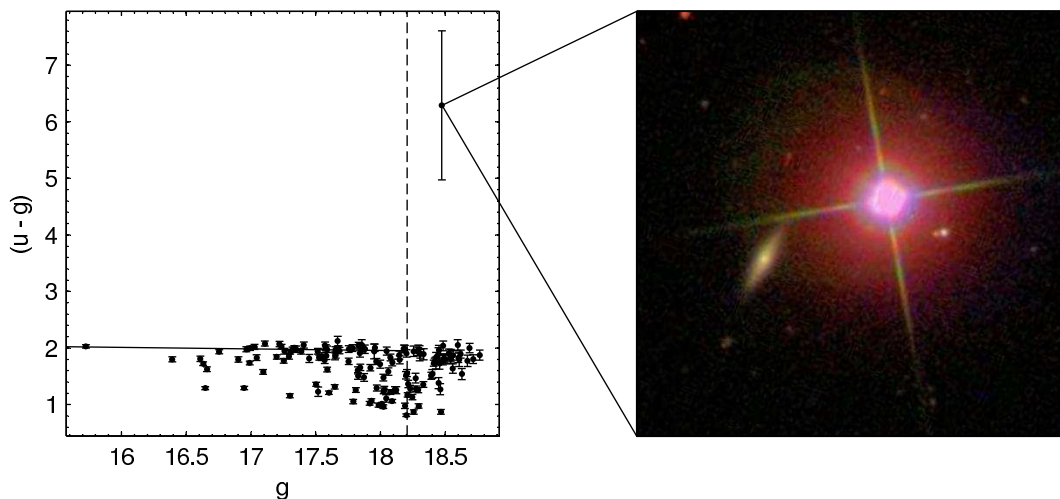


Figure 10. Discordant point on the $(u-g)$ versus g colour-magnitude diagram for Abell 971. A near-by saturated star affects the photometry of the target galaxy.

is due to superpositions of line-of-sight galaxies. A typical example is the discordant point on the $(g-i)$ versus i colour-magnitude diagram for Abell 1767 (Fig. 9). The same discordant point also lies far below the blue cloud in the $(u-i)$ versus i , and $(r-i)$ versus i colour-magnitude diagrams and far above the red sequence in the $(i-z)$ versus z plane.

Photometric saturation from a bright near-by stars also affects the photometry of a number of galaxies. Fig. 10 shows one such point on the $(u-g)$ versus g colour-magnitude diagram for Abell 971.

Dust reddening appears to affect other galaxies, as determined from a visual inspection of their image (i.e. obvious dust lanes). However, a unique set of galaxies in Abell 1809

appears to possess very red colours (Fig. 11). We were unable to determine the cause of these galaxies anomalous colours.

In total, the amount of contamination in the photometric galaxy catalogue is very small. Of the 10,529 galaxies, only 46 galaxies (or 0.4 per cent) have colours which are atypical (3σ above or 5σ below the mean galaxian colour of their host cluster). Of these 46 discordant points, 13 are due to line-of-sight galaxy effects (Fig. 9), 11 are due to saturation from nearby stars (Fig. 10), and 12 are suspected to be due to dust reddening, or the situation outlined in Fig. 11. The majority of the remaining discordant points appear to be genuinely blue galaxies. Of the 7 genuinely blue galaxy, 4 are spectroscopically confirmed low-redshift QSOs. There

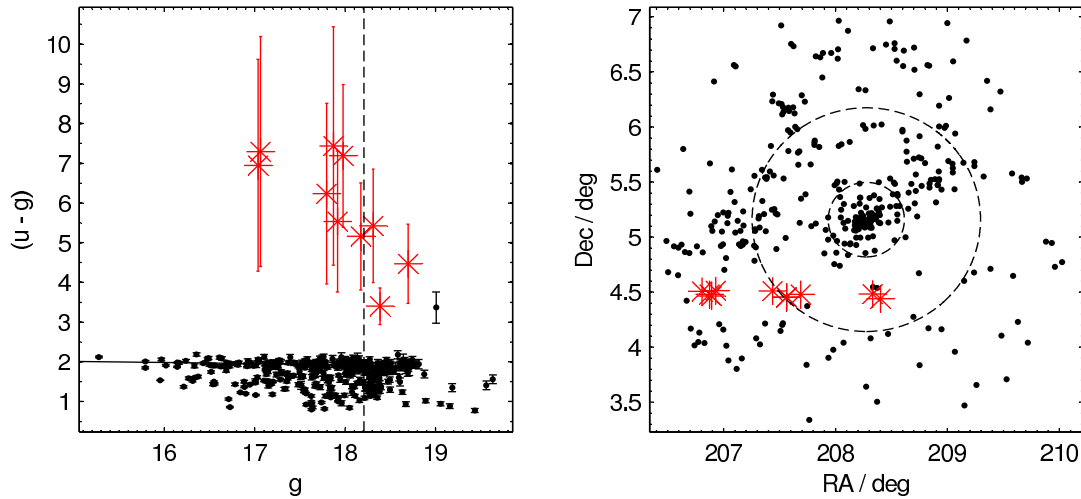


Figure 11. A series of discordant points in Abell 1809 that appear to congregate around 4.5 degrees of declination on the RA-Dec diagram. No bad pixel rows or nearby sources of photometric contamination have been found for these points. The tightness in Dec is suggestive of an observational artifact.

were also 2 genuinely red galaxies and 1 galaxy which was bifurcated at the edge of a stripe.

Given we have $\sim 10,000$ objects in our sample, we may have expected ~ 100 to have significantly unusual colours (by our above definition). Our 46 outliers is slightly fewer than this expectation value, but is not worrisome, particularly as we look for $> 5\sigma$ bluer than the mean galaxy colour to avoid the blue cloud.